

N 62 63263 325
Copy
RM L55D22

CONFIDENTIAL

NACA RM L55D22



**CASE FILE
COPY**

RESEARCH MEMORANDUM

EFFECTS OF SPANWISE LOCATION OF SWEEP DISCONTINUITY
ON THE LOW-SPEED STATIC LATERAL STABILITY
CHARACTERISTICS OF A COMPLETE MODEL
WITH WINGS OF M AND W PLAN FORM

By Paul G. Fournier

Langley Aeronautical Laboratory
Langley Field, Va.

CLASSIFICATION CHANGED TO UNCLASSIFIED
AUTHORITY: NACA RESEARCH ABSTRACT NO. 109
EFFECTIVE DATE: NOVEMBER 14, 1956

CLASSIFIED DOCUMENT

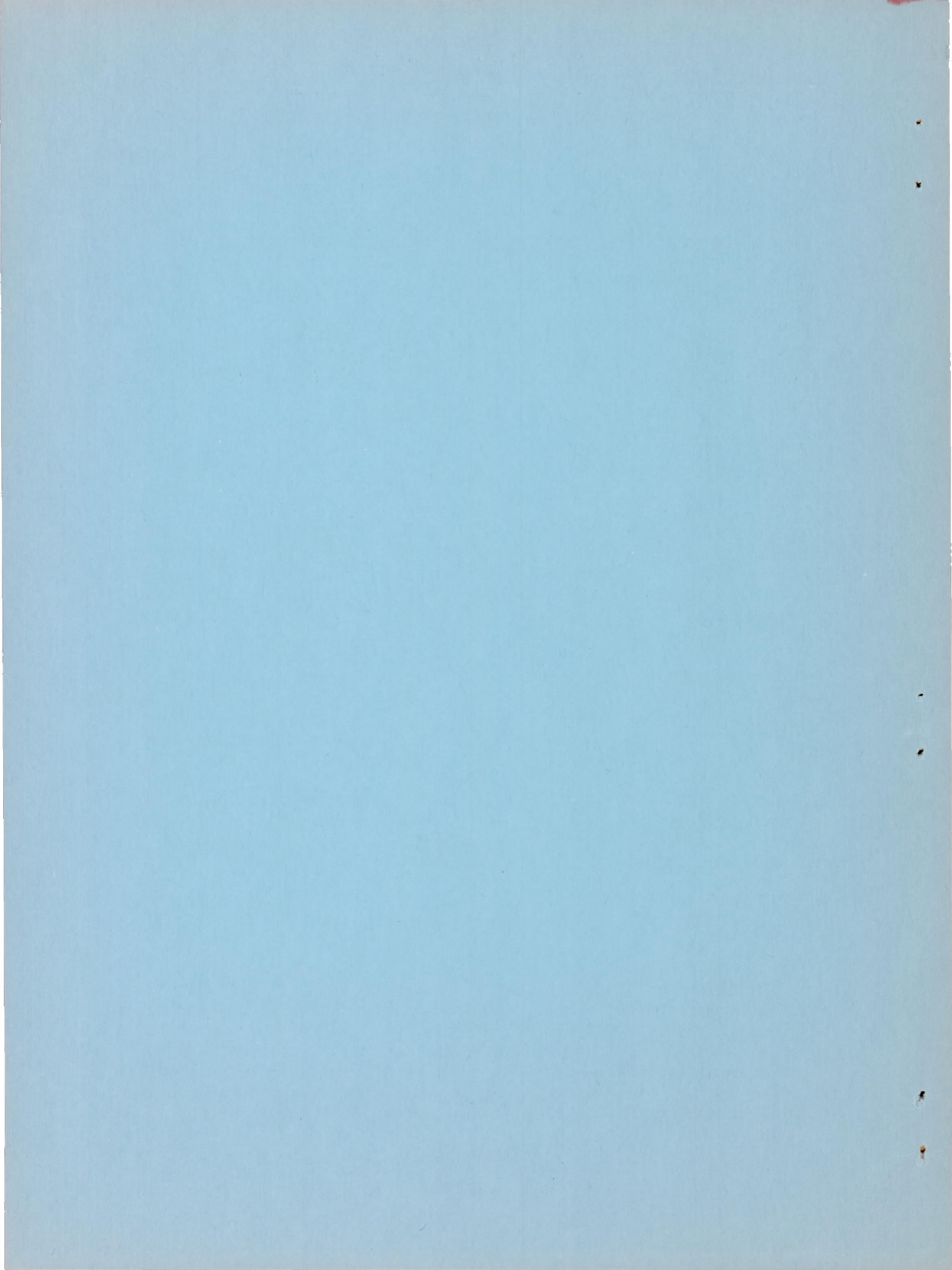
This material contains information affecting the National Defense of the United States within the meaning of the espionage laws, Title 18, U.S.C., Secs. 793 and 794, the transmission or revelation of which in any manner to an unauthorized person is prohibited by law.

NATIONAL ADVISORY COMMITTEE FOR AERONAUTICS

WASHINGTON

May 25, 1955

CONFIDENTIAL



NATIONAL ADVISORY COMMITTEE FOR AERONAUTICS

RESEARCH MEMORANDUM

EFFECTS OF SPANWISE LOCATION OF SWEEP DISCONTINUITY
ON THE LOW-SPEED STATIC LATERAL STABILITY
CHARACTERISTICS OF A COMPLETE MODEL
WITH WINGS OF M AND W PLAN FORM

By Paul G. Fournier

SUMMARY

An investigation was made of the low-speed static lateral stability characteristics of a complete model having a series of M- and W-wings. These wings were obtained through modification of a basic 45° swept wing and were designed to cover a range of spanwise location of the sweep discontinuity. All wings had an aspect ratio of 6, a taper ratio of 0.6, and 45° sweepforward or sweepback of the various wing panels.

The results indicate that, for the range of spanwise location of sweep discontinuity investigated (outboard of midsemispan for the W-wings and inboard of midsemispan for the M-wings), the variation of effective dihedral with spanwise location of sweep discontinuity was appreciable for the W-wings but was very small for the M-wings.

In general, all the configurations investigated with the M-wings and some of the configurations with the W-wings gave positive static directional stability over the lift-coefficient range investigated including the stall.

INTRODUCTION

In reference 1 it has been shown that the static longitudinal stability characteristics of a sweptback wing at high lift coefficients can be improved by modification of the wing to one of the composite (M or W) plan forms, that is, plan forms made up of combinations of sweptback and sweepforward panels. During the investigation reported in reference 1, the same series of M- and W-wings was tested in sideslip in order to determine the effect of spanwise location of sweep

CONFIDENTIAL

discontinuity on the static lateral stability characteristics. These results are presented herein. The M-wings tested had sweep discontinuities located at 30-percent, 40-percent, or 50-percent semispan; and the W-wings had sweep discontinuities located at 50-percent, 60-percent, or 70-percent semispan. All wings had an aspect ratio of 6, a taper ratio of 0.60, NACA 65A009 airfoil sections parallel to the plane of symmetry, and $\pm 45^\circ$ panel sweep of the quarter-chord lines.

The results of the static lateral stability tests are presented for conditions with the horizontal and vertical tails off and on and for two vertical locations of the horizontal tail. One location (referred to as the low tail) was on the wing chord plane extended, and the other location (referred to as the high tail) was at 20.83-percent wing semispan above the wing chord plane extended.

COEFFICIENTS AND SYMBOLS

The stability system of axes used for the presentation of the data and the positive direction of forces, moments, and angles are shown in figure 1. All moments are referred to the quarter-chord point of the wing mean aerodynamic chord.

A	aspect ratio
b	wing span, ft
C_L	lift coefficient, $\frac{\text{Lift}}{qS}$
C_l	rolling-moment coefficient, $\frac{\text{Rolling moment}}{qSb}$
C_n	yawing-moment coefficient, $\frac{\text{Yawing moment}}{qSb}$
C_Y	lateral-force coefficient, $\frac{\text{Lateral force}}{qS}$
$C_{l\beta}$	rolling moment due to sideslip per degree, $\partial C_l / \partial \beta$
$C_{n\beta}$	yawing moment due to sideslip per degree, $\partial C_n / \partial \beta$
$C_{Y\beta}$	lateral force due to sideslip per degree, $\partial C_Y / \partial \beta$

$$C_{l\beta C_L} = \frac{\partial \frac{\partial C_L}{\partial \beta}}{\partial C_L}$$

\bar{c}	wing mean aerodynamic chord, ft
\bar{c}_t	horizontal-tail mean aerodynamic chord, ft
D	diameter of fuselage, in.
l_F	fuselage length, in.
l_t	tail length, distance from $\bar{c}/4$ to $\bar{c}_t/4$, ft
q	free-stream dynamic pressure, $\rho V^2/2$, lb/sq ft
S	wing area, sq ft
S_t	horizontal-tail area, sq ft
V	free-stream velocity, ft/sec
\bar{x}	chordwise distance from leading edge of root chord to $\bar{c}/4$ (positive rearward of leading edge), in.
y	distance from plane of symmetry to any spanwise station, ft
y^*	lateral location of sweep discontinuity, percent $b/2$
α	angle of attack, deg
β	angle of sideslip, deg
$\Lambda_{c/4}$	sweep of quarter-chord line, deg
ρ	mass density of air, slugs/cu ft

Notation:

Λ	basic sweptback wing
M or W	composite plan-form wings (used with subscript 30, 40, 50, 60, or 70 indicating spanwise location of sweep discontinuity in percent $b/2$)
F	fuselage

V	vertical tail
H _H	horizontal tail, high
H _L	horizontal tail, low
W	wing

MODEL AND APPARATUS

For the present investigation, a series of seven plan forms were tested - each in combination with a fuselage and tail. The wings are the same as those presented in reference 1. The wings had an aspect ratio of 6, a taper ratio of 0.60, an NACA 65A009 airfoil section parallel to the plane of symmetry, and 45° sweepback or sweepforward of the quarter-chord lines. The wings include a sweptback wing (basic, $\Lambda_c/4 = 45^\circ$), three M-wings, and three W-wings. The three M-wings had their sweep discontinuities located at 30-percent, 40-percent, and 50-percent semispan; whereas the three W-wings had sweep discontinuities at 50-percent, 60-percent, and 70-percent semispan. These wings are designated as M₃₀, M₄₀, M₅₀, W₅₀, W₆₀, and W₇₀ wings, respectively. The horizontal tail has an aspect ratio of 4, a taper ratio of 0.60, 45° sweepback of the quarter-chord line, and NACA 65A006 airfoil sections parallel to the plane of symmetry. The fuselage has a fineness ratio of 10.86 which was achieved by cutting off a portion of the rear of a fineness-ratio-12 closed body of revolution, the ordinates of which are presented in reference 1. The fuselage was constructed of wood and the wings were constructed of wood bonded to steel reinforcing spars. A three-view drawing of the model with a representative wing is shown in figure 2. A photograph of a typical complete-model configuration on the support strut is presented in figure 3.

All the wings tested in this investigation are in a midwing position and are mounted so that the quarter-chord point of the wing mean aerodynamic chord, about which all moments and forces are taken, is located at the same point on the fuselage for all the wings. Details of these wing plan forms are presented in figure 4. The model was constructed so that tests could be made with the horizontal tail at two tail heights. The high tail was located 20.83-percent wing semispan above the wing chord plane extended and the low tail was on the wing chord plane extended.

The model was mounted on a single support strut, which in turn was attached to the mechanical balance system of the Langley 300 MPH 7- by 10-foot tunnel.

TESTS AND CORRECTIONS

All tests were made at a dynamic pressure of 45.22 pounds per square foot which for average test conditions corresponds to a Mach number of about 0.17 and a Reynolds number of 1,270,000 based on the wing mean aerodynamic chord of 1.02 feet.

The present investigation consists of tests made to determine the lateral characteristics of the model. The parameters $C_{l\beta}$, $C_{n\beta}$, and $C_{Y\beta}$ were determined from tests at sideslip angles of $\pm 5^\circ$ through the angle-of-attack range from approximately -4° to 32° . The angles of attack were corrected for jet-boundary effects and were computed on the basis of unswept-wing theory by the method of reference 2. Reference 3 shows that the effect of sweep on this correction is small. The dynamic pressure has been corrected for blocking, caused by the model and its wake, by the method of reference 4.

Vertical buoyancy on the support strut, tunnel air-flow misalignment, and longitudinal pressure gradient have been accounted for in the computation of the data. These data have not been corrected for the tares caused by the model support strut; however, tare tests of a similar complete-model configuration have indicated that the tares corresponding to the lateral coefficients are small.

RESULTS AND DISCUSSION

Presentation of Results

The results of the present investigation are presented in the following figures:

	<u>Figure</u>
Basic data	5 to 12
Effect of spanwise location of sweep discontinuity on $C_{l\beta}$. .	13
Variation of $C_{l\beta C_L}$ with spanwise location of sweep discontinuity	14
Effect of spanwise location of sweep discontinuity on $C_{n\beta}$. .	15
Effect of spanwise location of sweep discontinuity on $C_{Y\beta}$. .	16

Lateral Stability Characteristics

Rolling moment due to sideslip.- The static lateral stability derivatives for the wing-fuselage configuration (fig. 13(a)) indicate, in general, that the effective-dihedral characteristics of the M-wings are similar to those of the swept wing. The M-wings indicate relatively little effect of spanwise location of sweep discontinuity on $C_{l\beta}$ - probably because the changes in area involved, as the location of sweep discontinuity was moved inboard of $y^* = 50$, had small moment arms. The characteristics of the W_{50} wing is more like the characteristics that would be expected for a sweptforward wing (ref. 5), probably because the sweptforward portion of the W_{50} wing has the greatest moment arm. However, a reduction in the span of the sweptforward portions of these W-wings allows the effective dihedral to approach that of the sweptback wing, probably because the considerably larger areas of the sweptback portions of the wing offset the effect of the greater moment arm of the sweptforward portions of the wing.

The lateral stability characteristics of the model with wing off are shown in figure 12. The results indicate that the contribution of the fuselage to $C_{l\beta}$ is negligible. The vertical-tail contribution to $C_{l\beta}$ decreased with increasing angle of attack, which probably is due in part to the fact that the force on the vertical tail moves toward the roll axis with increasing angle of attack. The general trend of $C_{l\beta}$ with y^* (fig. 13) of the complete-model configurations, as well as the complete model less the horizontal tail, is the same as that of the wing-fuselage configuration and indicates that the sidewash effect is small. Within the range of horizontal-tail height investigated, there is little effect of tail height on $C_{l\beta}$, except at the higher lift coefficients. (See figs. 5 to 11.)

Within the range of spanwise location of sweep discontinuity investigated, figure 14 shows that the W-wings afford a greater range of $C_{l\beta C_L}$ than do the M-wings. The experimental wing-fuselage data for the basic sweptback wing are in good agreement with the theoretical results of reference 6.

Yawing moment due to sideslip.- Results for the wing-fuselage configurations (fig. 15(a)) indicate, in general, that there is very little effect of the plan-form variations investigated on $C_{n\beta}$, except at the high lift coefficients where both the M- and W-wing configurations eliminated static directional instability noted for the swept-wing configuration. For all the wing-fuselage configurations, the fuselage produces almost the entire amount of directional instability up to maximum lift coefficient, as may be seen by comparing the wing-fuselage data of figure 15(a) with the fuselage-alone data of figure 12.

Comparison of figure 15(b) (WFV) with figure 15(a) (WF) shows that the contribution of the vertical tail to $C_{n\beta}$ is relatively independent of spanwise location of sweep discontinuity for either the M- or W-wings.

Comparison of the data for the complete-model configurations $WFVH_H$ of figure 15(c) and $WFVH_L$ of figure 15(d) with results for the horizontal-tail off (fig. 15(b)) indicates that the addition of the horizontal tail, at either of the heights investigated, had no appreciable effect on directional stability. In general, all the configurations investigated with the M-wings and some of the configurations with the W-wings gave positive static directional stability over the lift-coefficient range investigated, including the stall.

Lateral force due to sideslip.- Results for the wing-fuselage configurations (fig. 16(a)) indicate, in general, that there is very little effect of the plan-form variations investigated on lateral force due to sideslip $C_{Y\beta}$. Also, for the wing-fuselage configurations, almost the entire value of $C_{Y\beta}$ is produced by the fuselage up to maximum lift coefficient, as may be seen by comparing the wing-fuselage data of figure 16(a) with the fuselage-alone data of figure 12.

CONCLUSIONS

Results of a low-speed wind-tunnel investigation of a complete-model configuration having M- and W-wings with varying spanwise locations of sweep discontinuity indicate the following conclusions:

1. For the ranges of spanwise location of sweep discontinuity investigated (outboard of midsemispan for W-wings and inboard of midsemispan for M-wings), the variation of effective dihedral with location of sweep discontinuity was appreciable for the W-wings but was very small for the M-wings.

2. In general, all the configurations investigated with the M-wings and some of the configurations with the W-wings gave positive static directional stability over the lift-coefficient range investigated including the stall.

3. None of the lateral stability characteristics were appreciably affected by addition of the horizontal tail in either of the two positions used.

Langley Aeronautical Laboratory,
National Advisory Committee for Aeronautics,
Langley Field, Va., March 30, 1955.

REFERENCES

1. Fournier, Paul G.: Effects of Spanwise Location of Sweep Discontinuity on the Low-Speed Longitudinal Stability Characteristics of a Complete Model With Wings of M and W Plan Form. NACA RM L54K23, 1955.
2. Gillis, Clarence L., Polhamus, Edward C., and Gray, Joseph L., Jr.: Charts for Determining Jet-Boundary Corrections for Complete Models in 7- by 10-Foot Closed Rectangular Wind Tunnels. NACA WR L-123, 1945. (Formerly NACA ARR L5G31.)
3. Polhamus, Edward C.: Jet-Boundary-Induced-Upwash Velocities for Swept Reflection-Plane Models Mounted Vertically in 7- by 10-Foot, Closed, Rectangular Wind Tunnels. NACA TN 1752, 1948.
4. Herriot, John G.: Blockage Corrections for Three-Dimensional-Flow Closed-Throat Wind Tunnels, With Consideration of the Effect of Compressibility. NACA Rep. 995, 1950. (Supersedes NACA RM A7B28.)
5. Purser, Paul E., and Spearman, M. Leroy: Wind-Tunnel Tests at Low Speed of Swept and Yawed Wings Having Various Plan Forms. NACA TN 2445, 1951. (Supersedes NACA RM L7D23.)
6. Polhamus, Edward C., and Sleeman, William C., Jr.: The Rolling Moment Due to Sideslip of Swept Wings at Subsonic and Transonic Speeds. NACA RM L54L01, 1955.

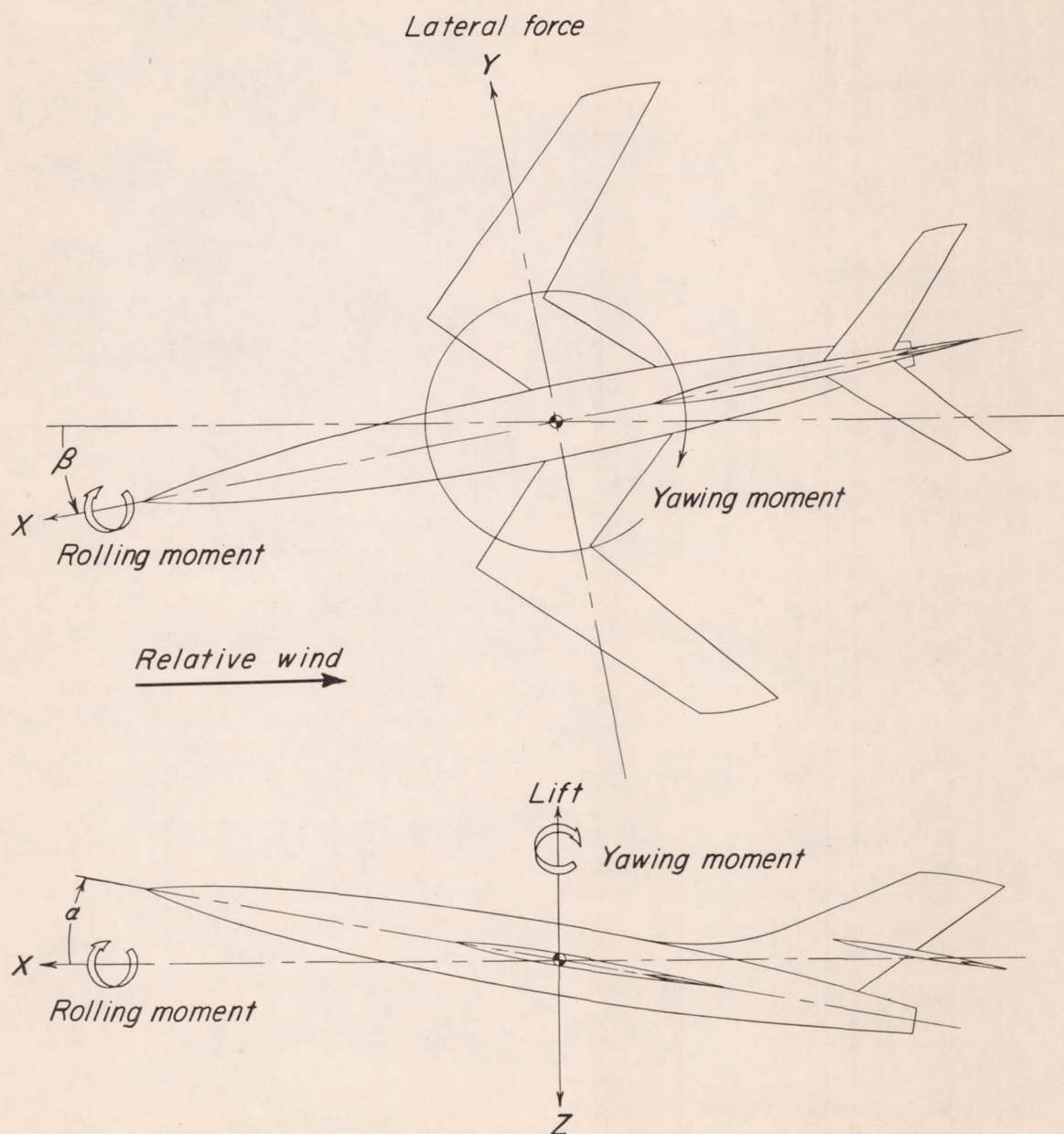
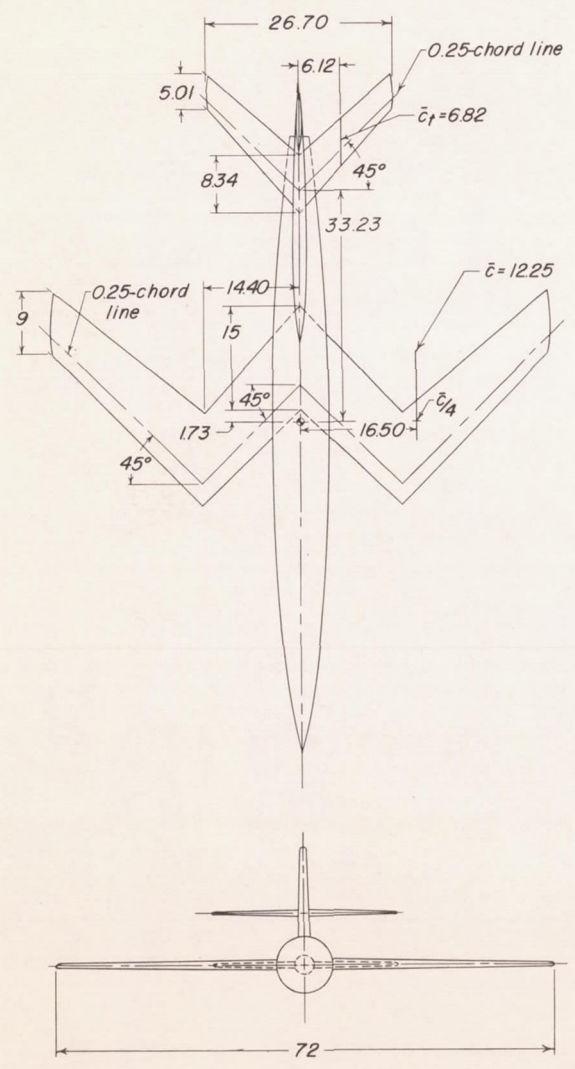


Figure 1.- Stability system of axes showing positive direction of forces, moments, and angles.



Physical Characteristics

Wing:

Sweep of $C_{1/4}$ inboard panel, deg	-45
Sweep of $C_{1/4}$ outboard panel, deg	45
Area, sq ft	6
Span, ft	6
Aspect ratio	6
Taper ratio	0.60
Mean aerodynamic chord, ft	1.02
Incidence, deg	0
Dihedral, deg	0
Airfoil section parallel to plane of symmetry	65A009

Horizontal tail:

Area, sq ft	1.24
Aspect ratio	4.00
Airfoil section parallel to plane of symmetry	NACA 65A006

Vertical tail:

Area, sq ft	1.69
Aspect ratio	1.18
Airfoil section parallel to plane of symmetry	63A009

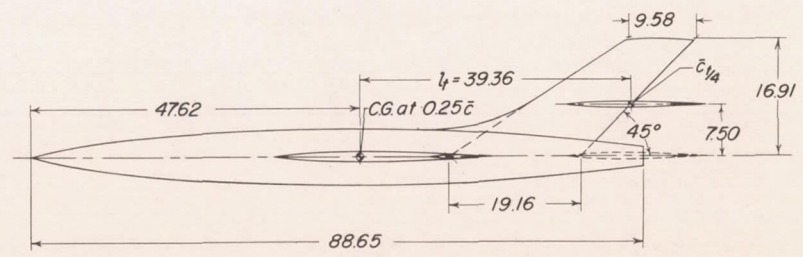
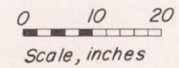


Figure 2.- General arrangement of test model with typical M-wing.



L-68568

Figure 3.- Photograph of typical model on support strut.

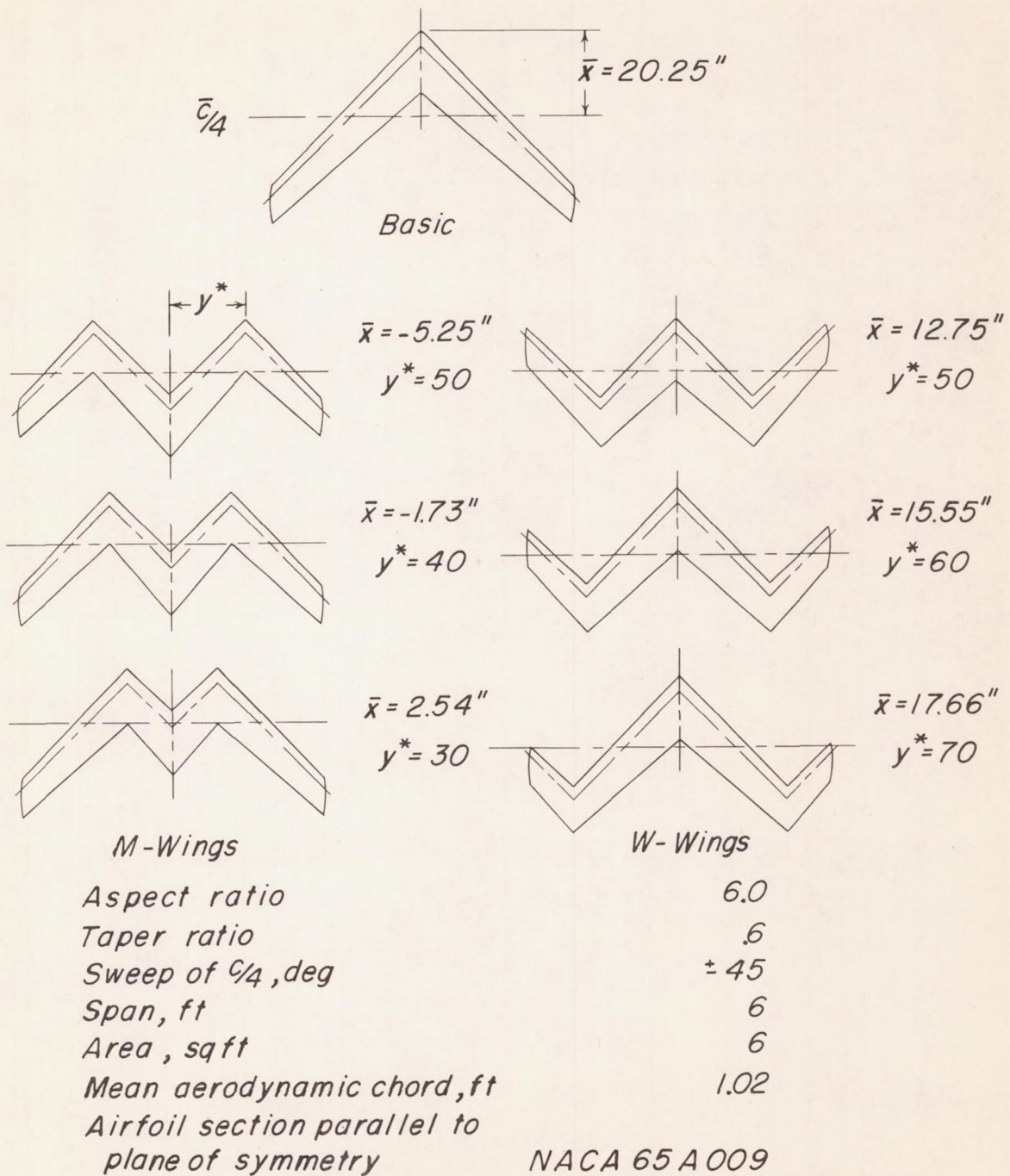


Figure 4.- Details of the various composite wings.

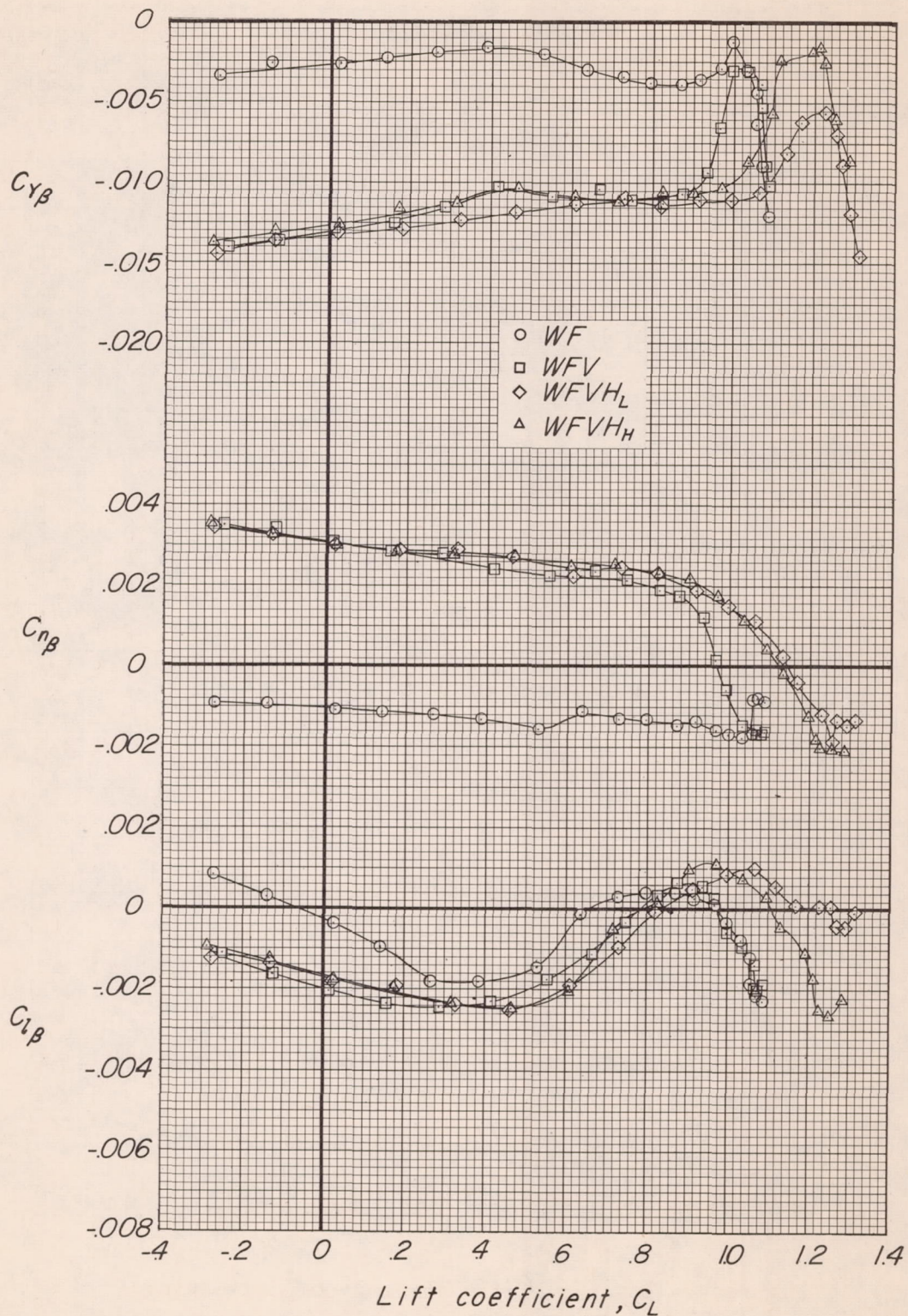


Figure 5.- Effect of component parts on the lateral stability characteristics of the model with the 45° swept wing (Δ).

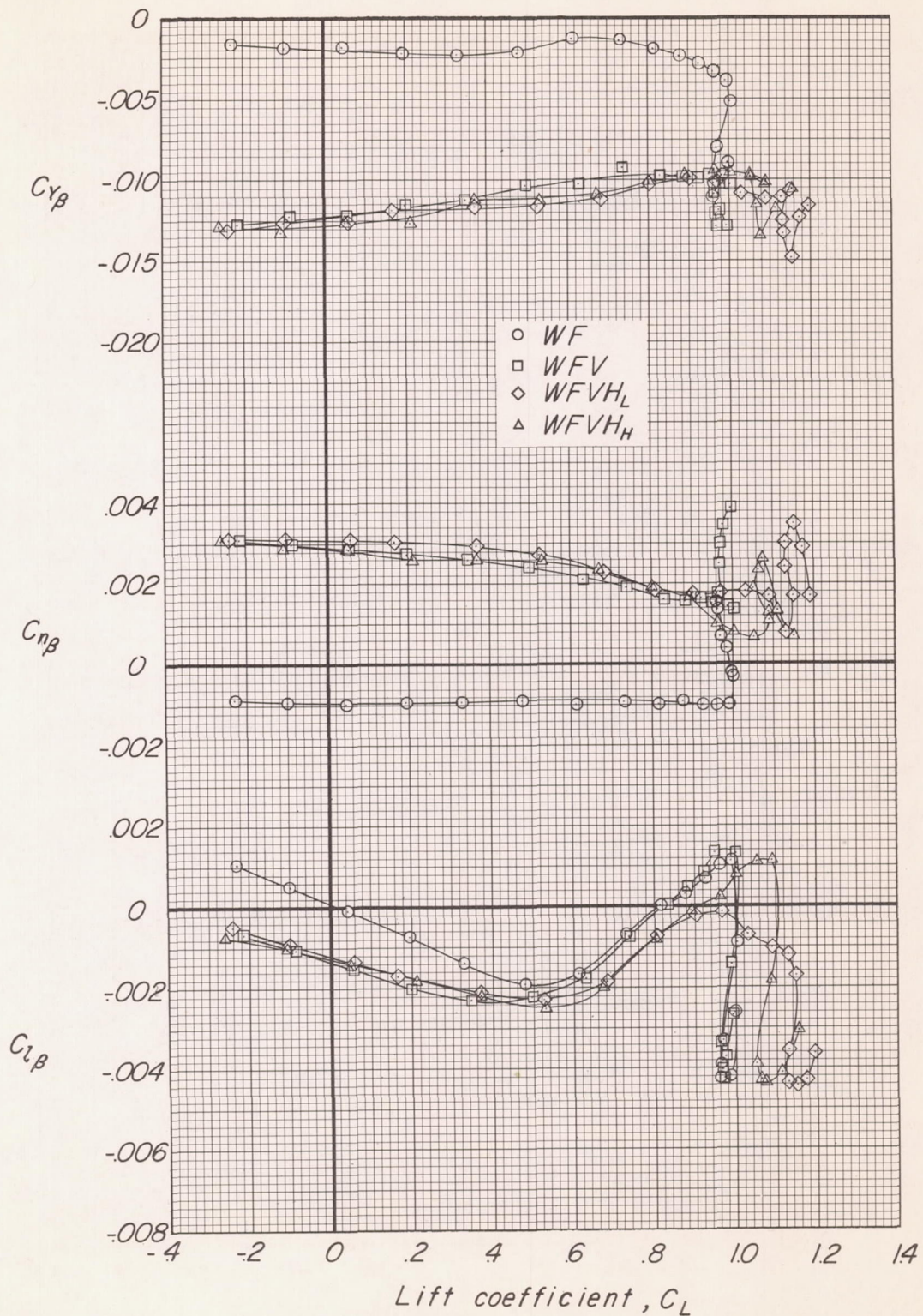


Figure 6.- Effect of component parts on the lateral stability characteristics of the model with the M₃₀ wing.

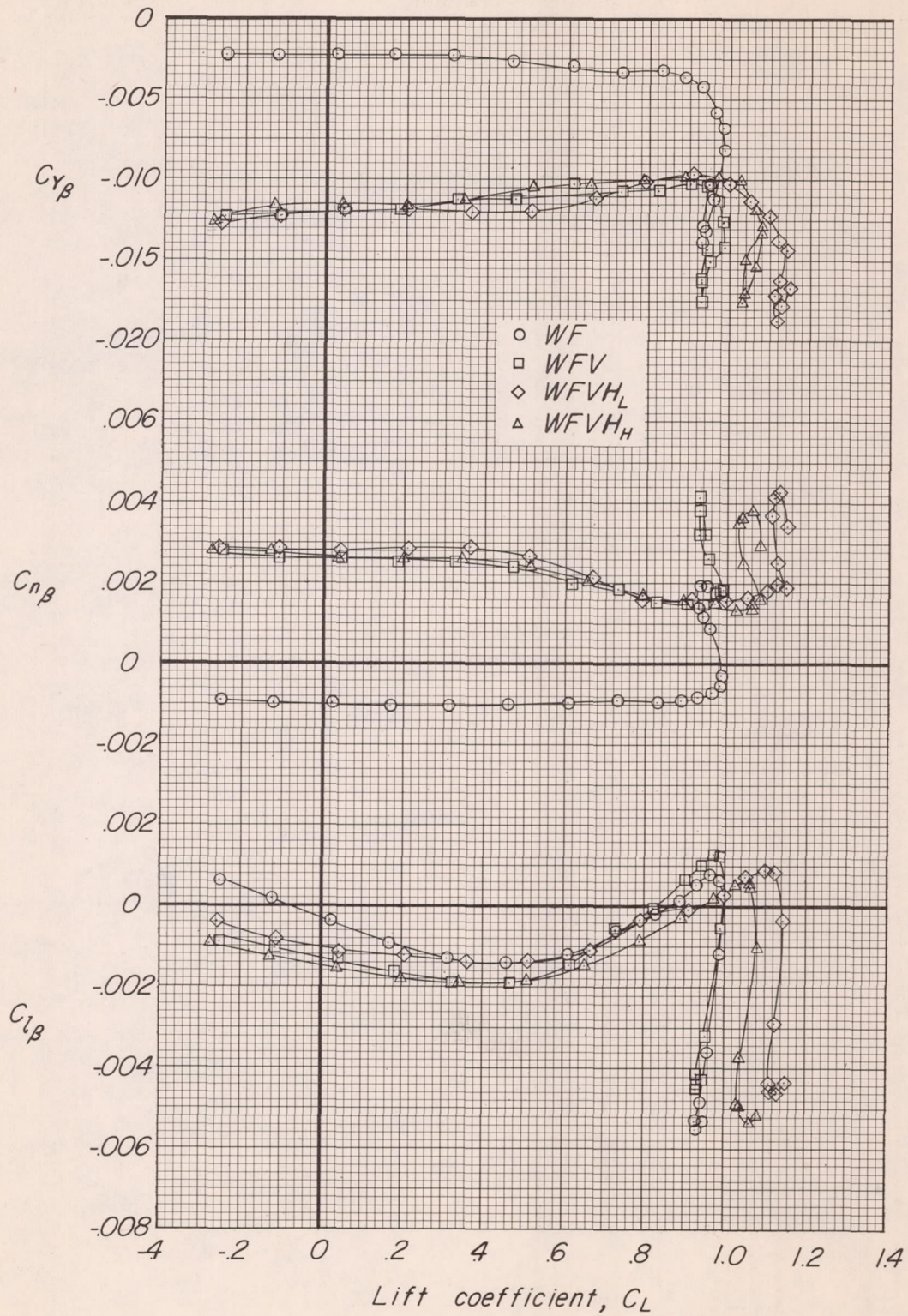


Figure 7.- Effect of component parts on the lateral stability characteristics of the model with the M_{40} wing.

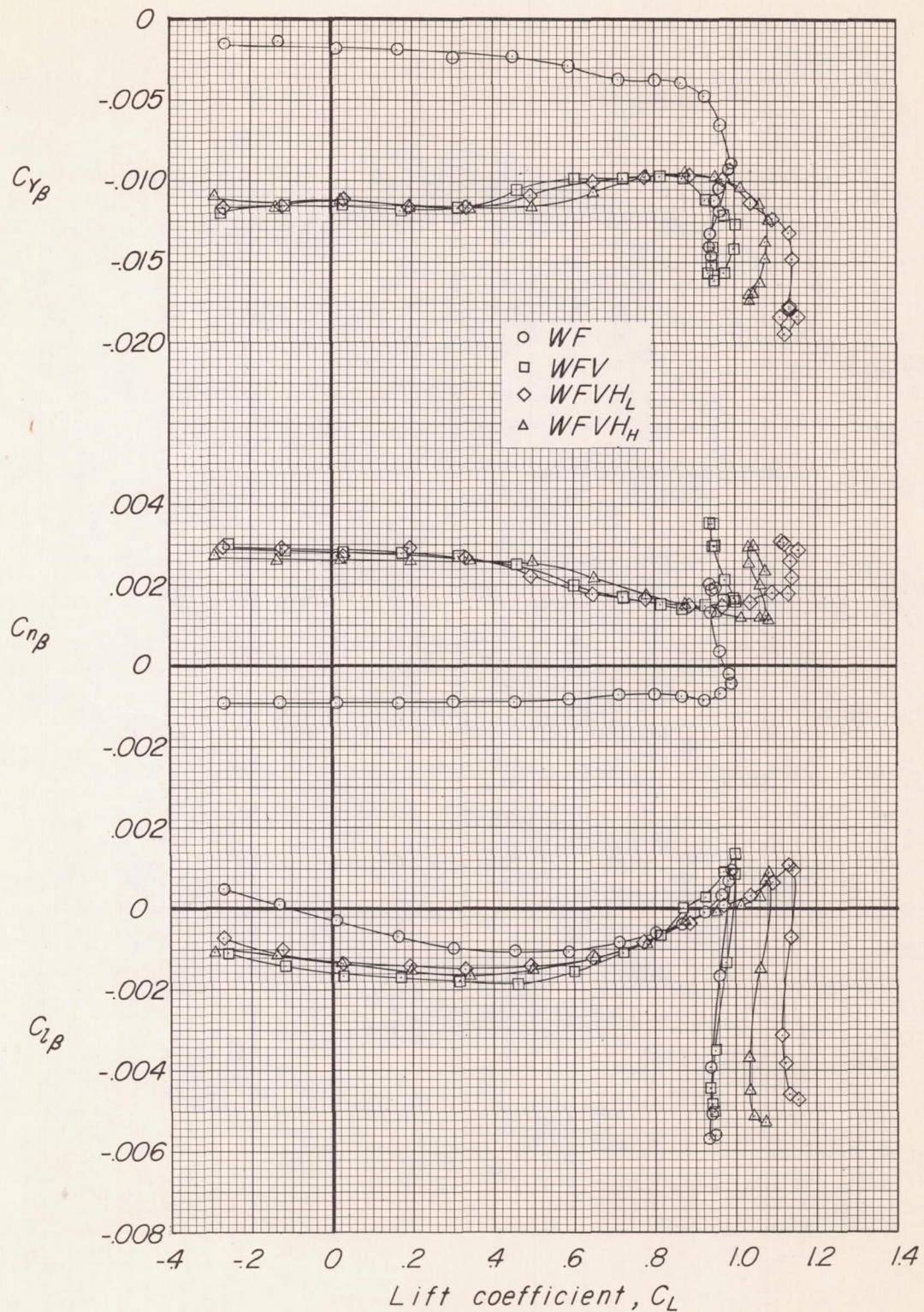


Figure 8.- Effect of component parts on the lateral stability characteristics of the model with the M₅₀ wing.

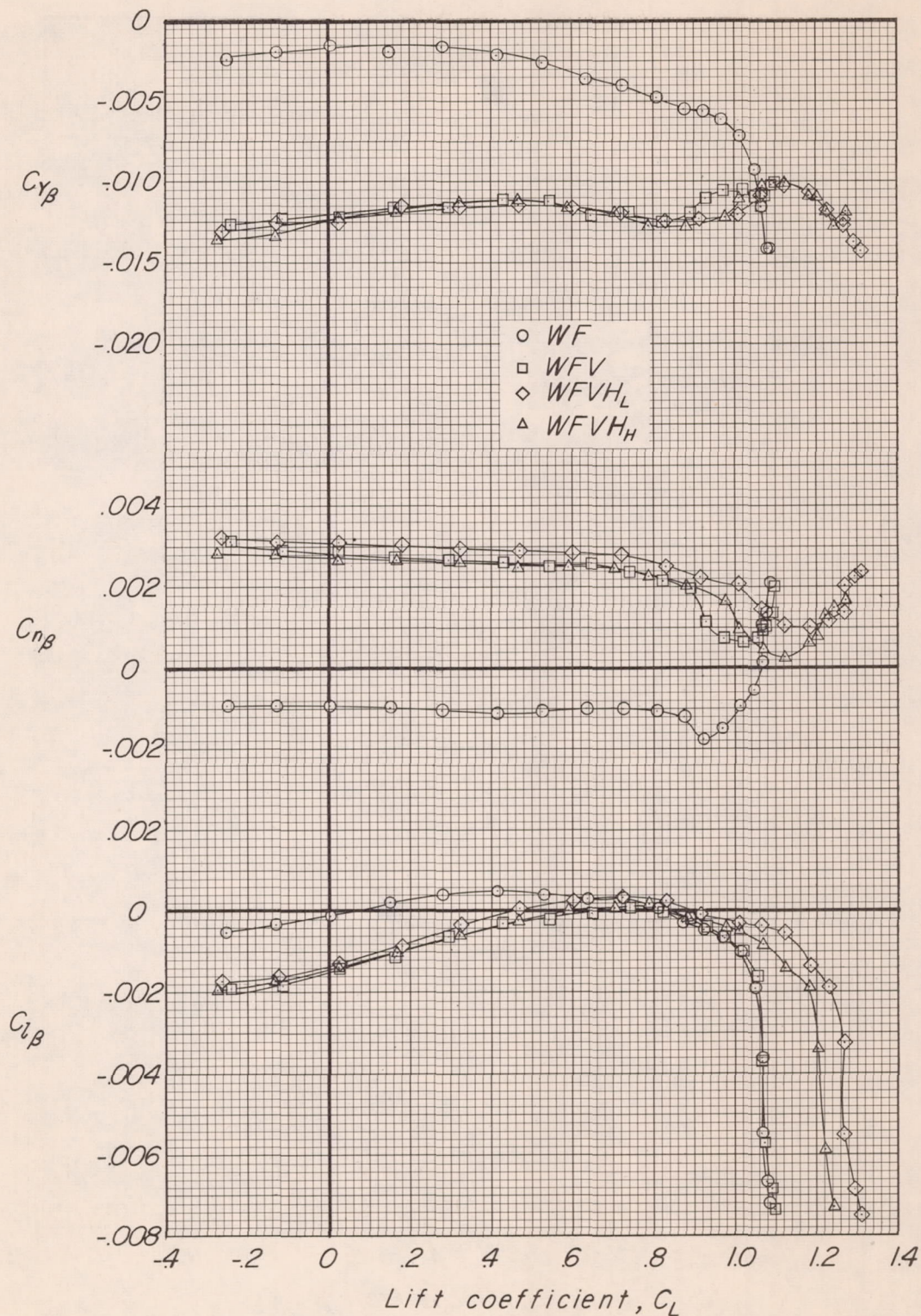


Figure 9.- Effect of component parts on the lateral stability characteristics of the model with the W_{50} wing.

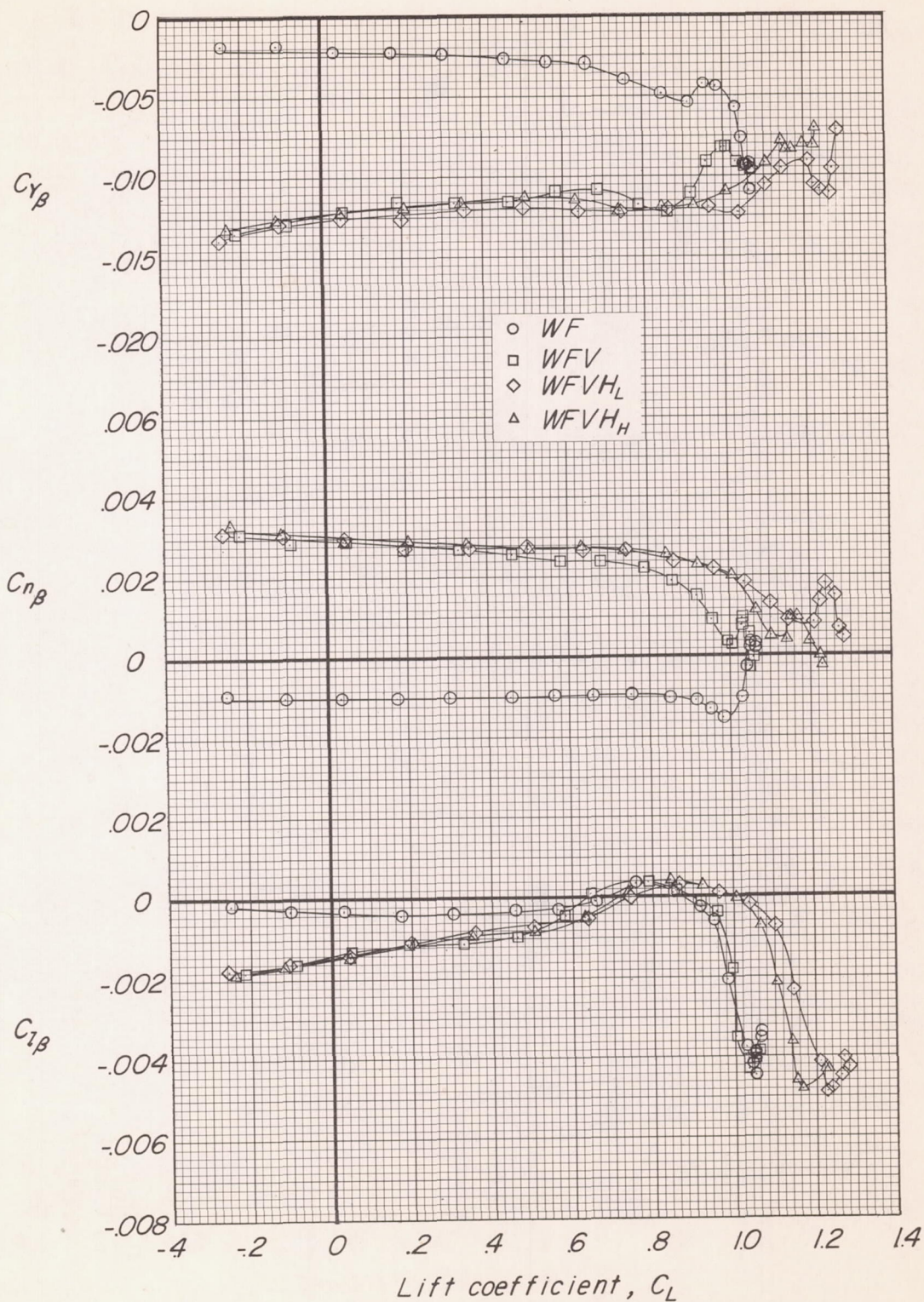


Figure 10.- Effect of component parts on the lateral stability characteristics of the model with the W₆₀ wing.

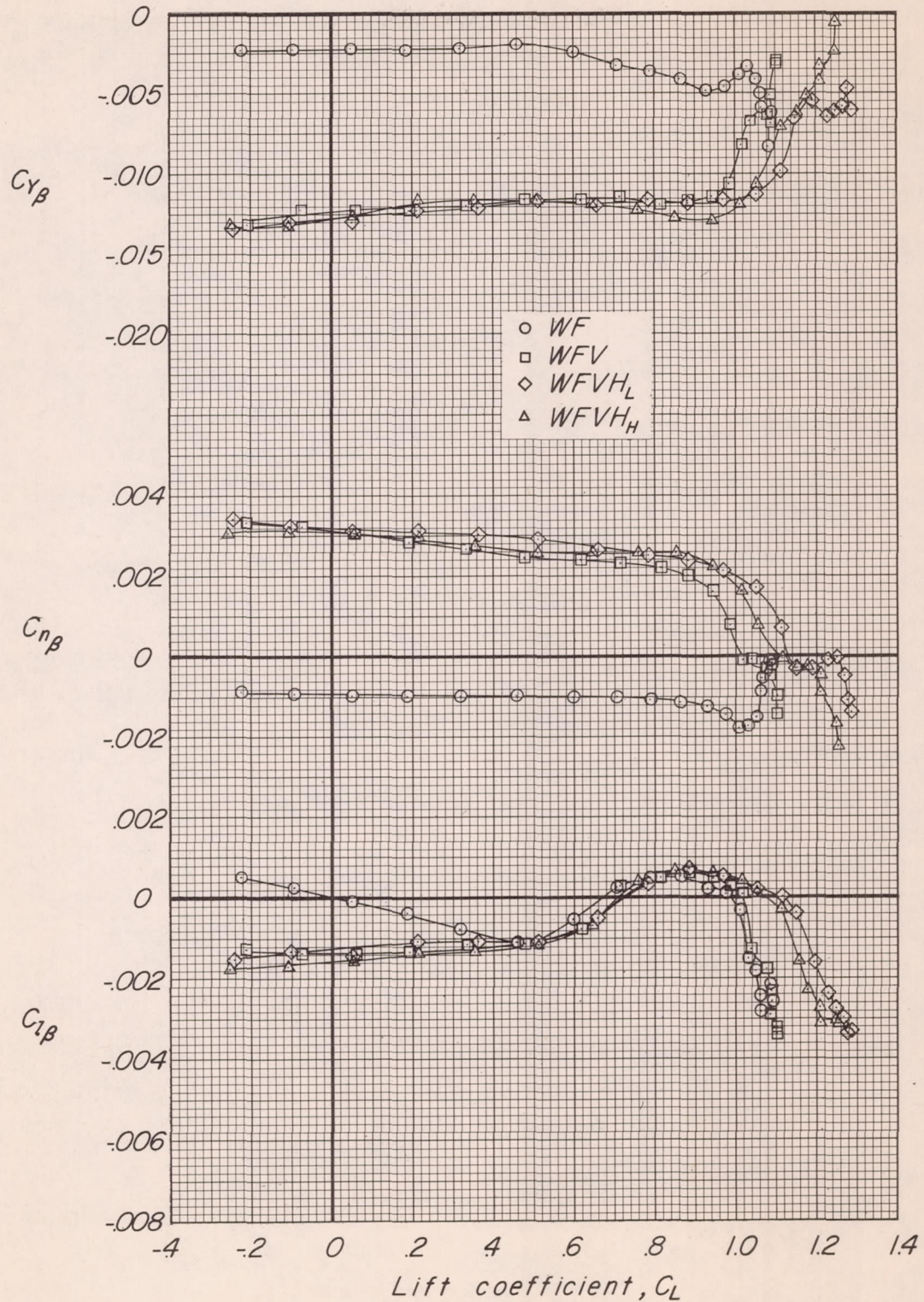


Figure 11.- Effect of component parts on the lateral stability characteristics of the model with the W70 wing.

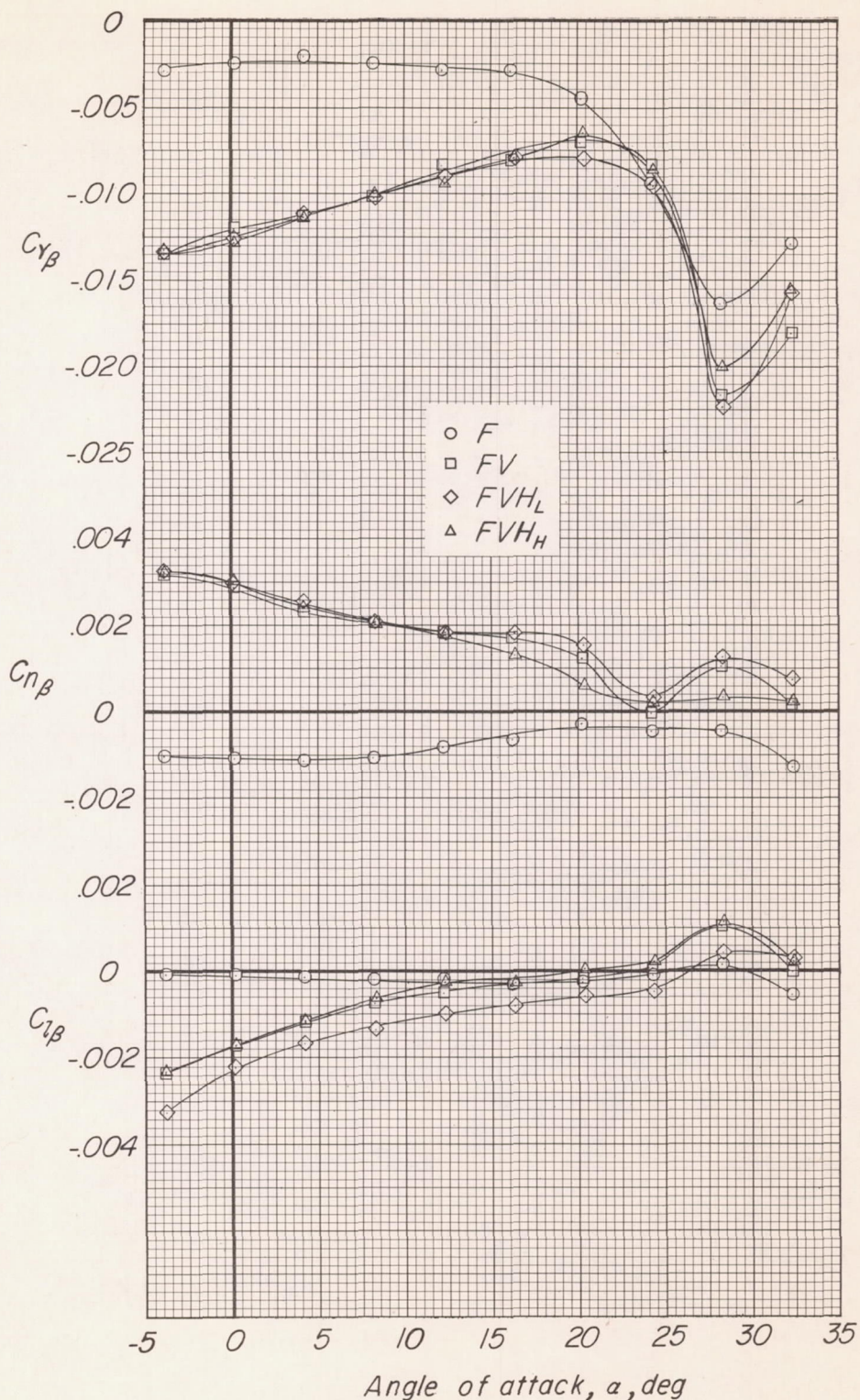
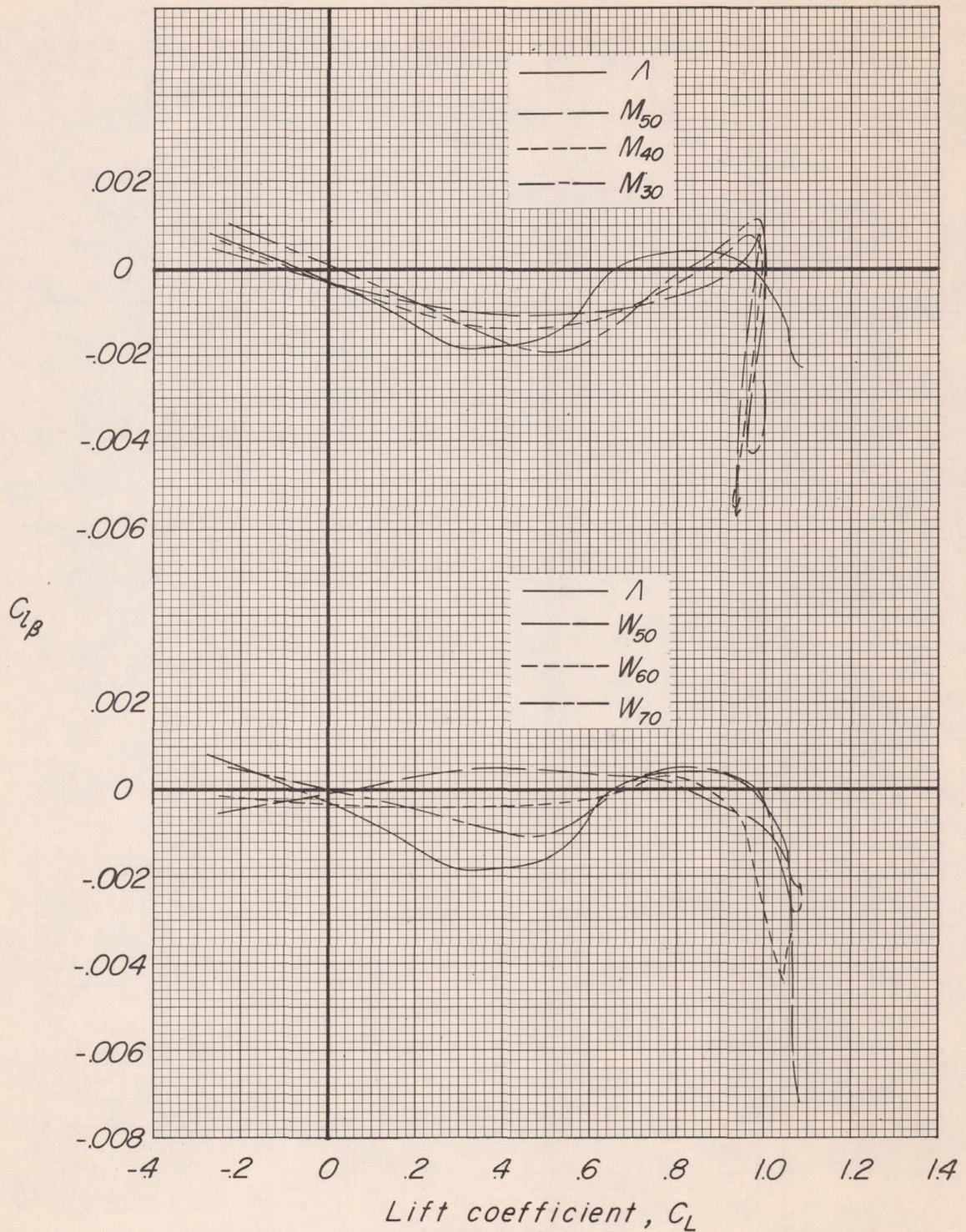
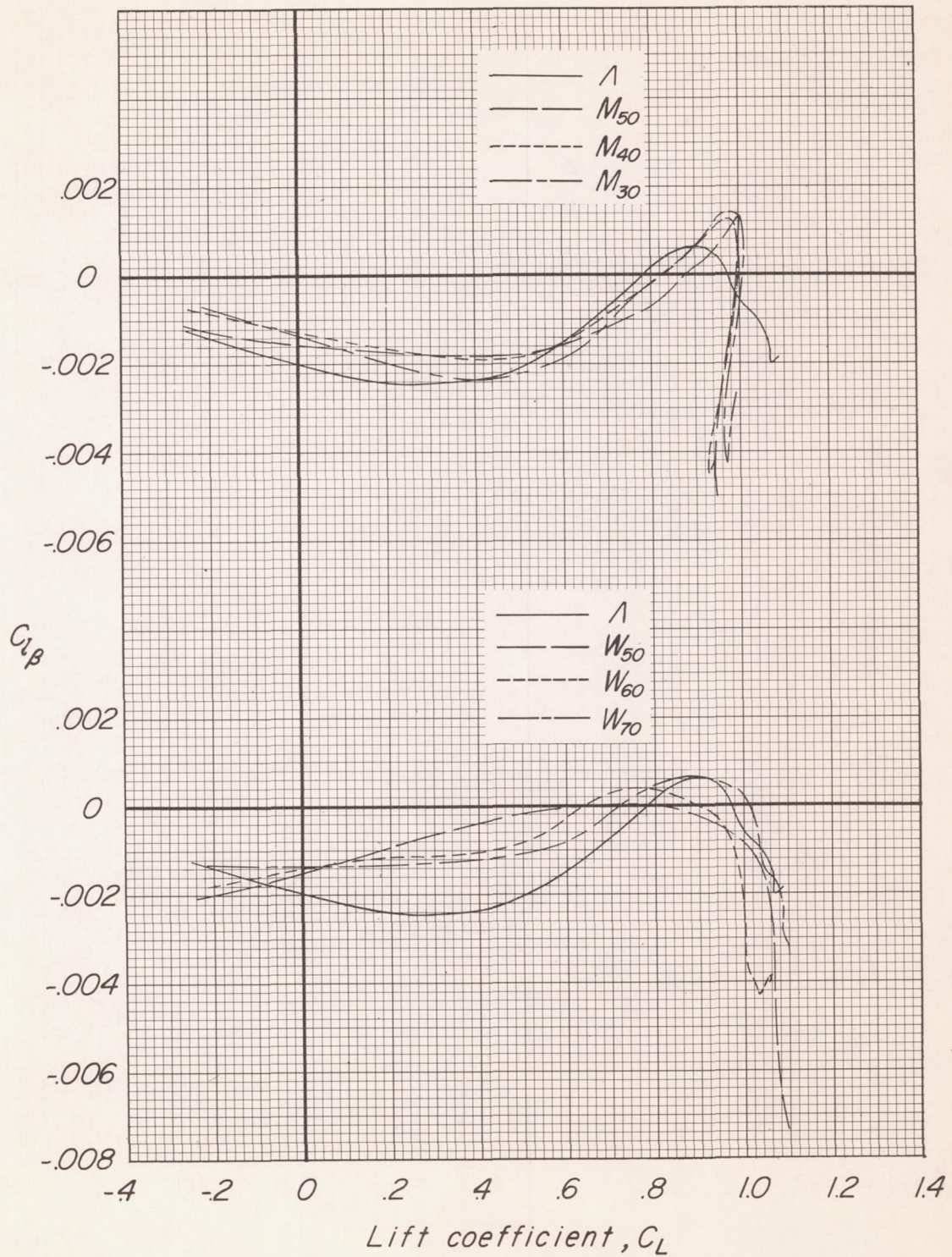


Figure 12.- Effect of component parts on the lateral stability characteristics of the model without a wing.



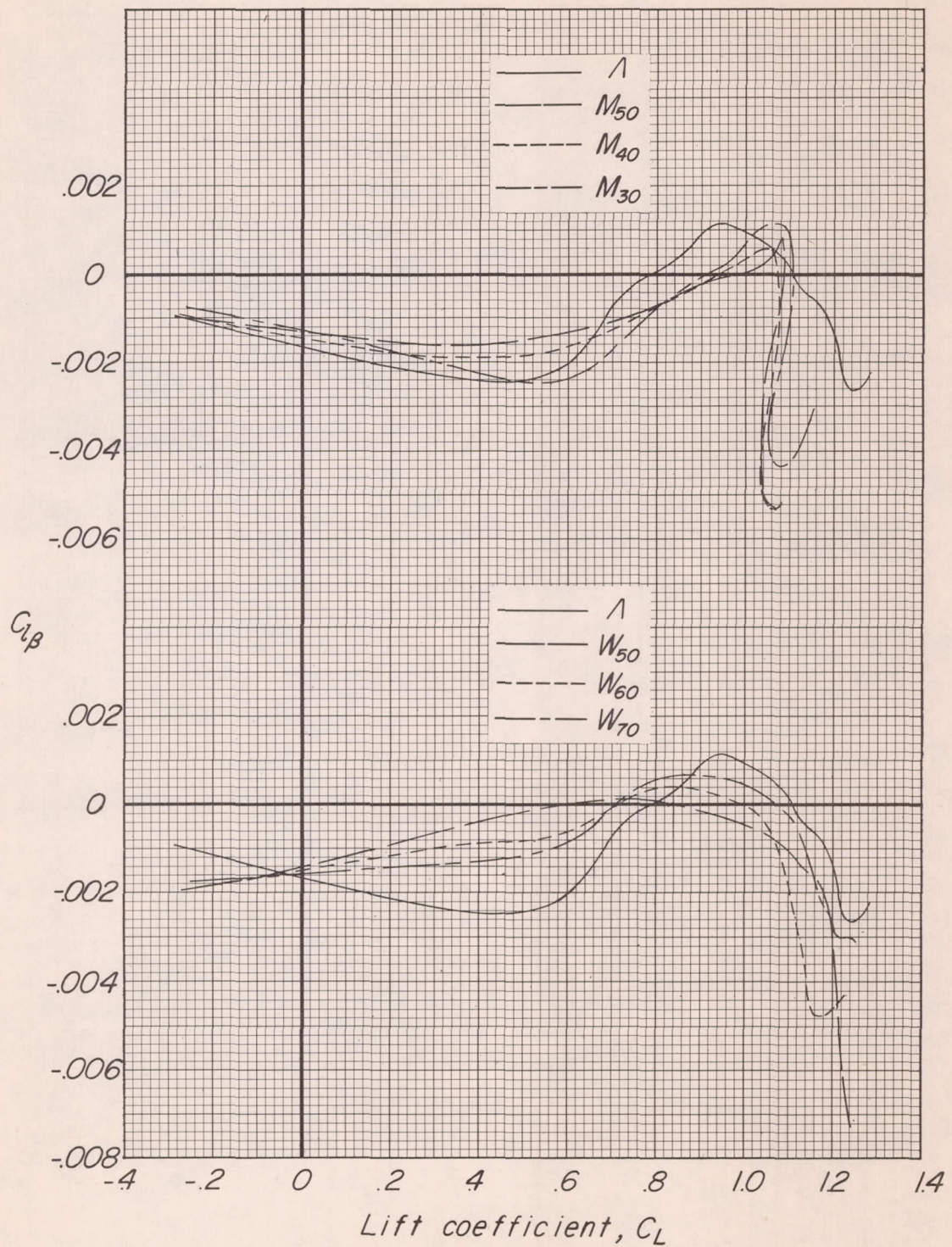
(a) WF.

Figure 13.- Effect of spanwise location of sweep discontinuity on rolling moment due to sideslip.



(b) WFV.

Figure 13.- Continued.



(c) W_{FVH_H}.

Figure 13.- Continued.

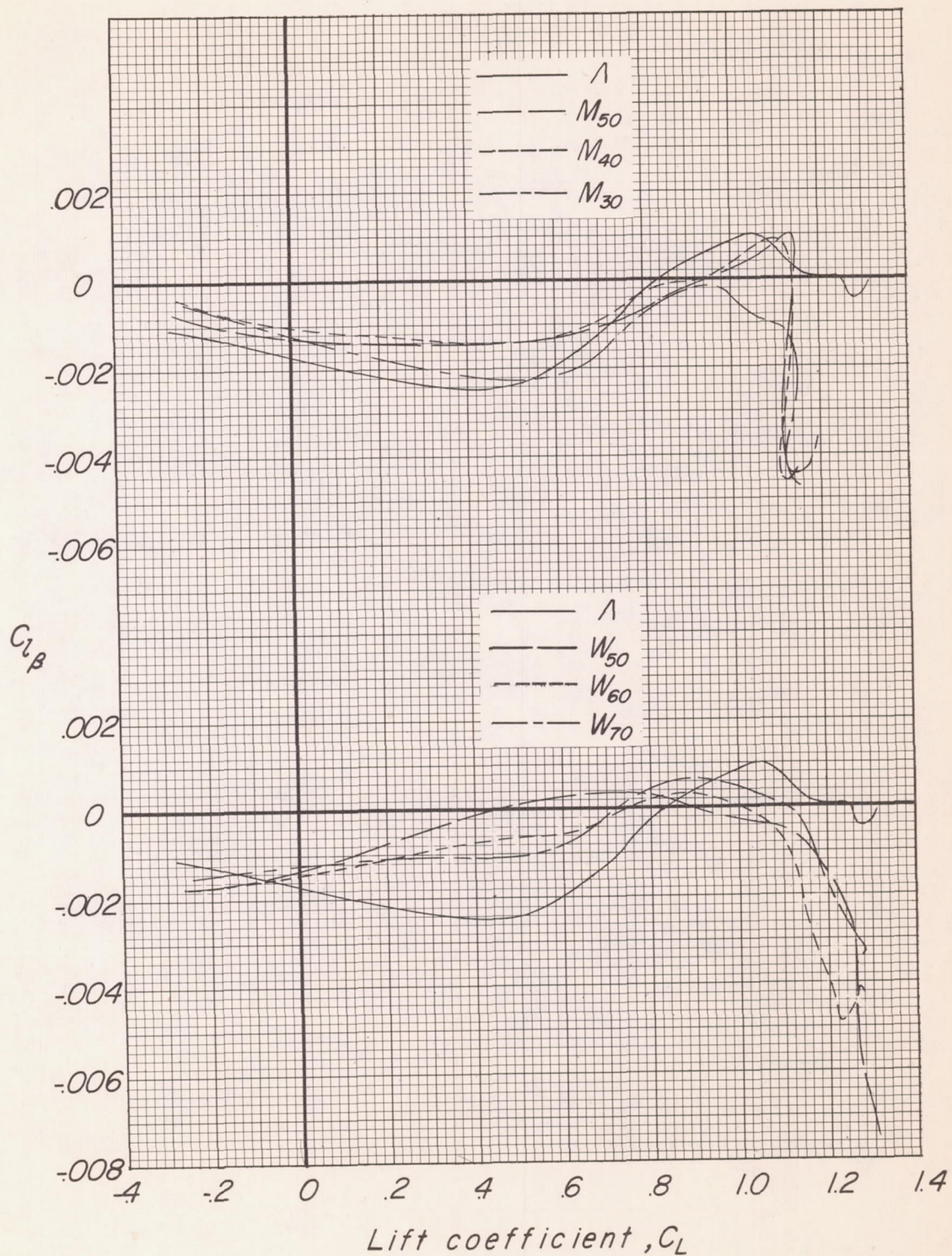
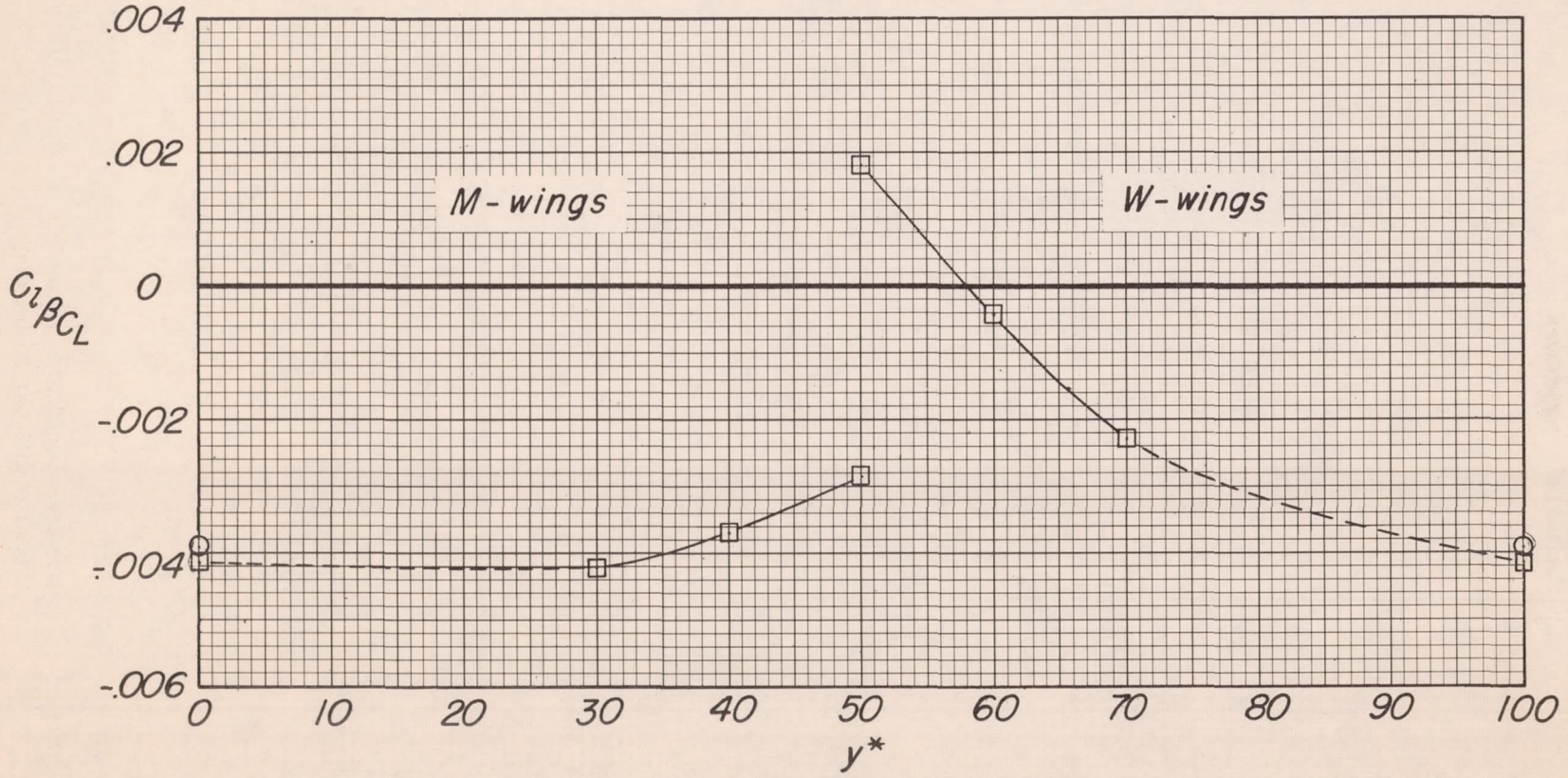
(d) W_{FVH_L}.

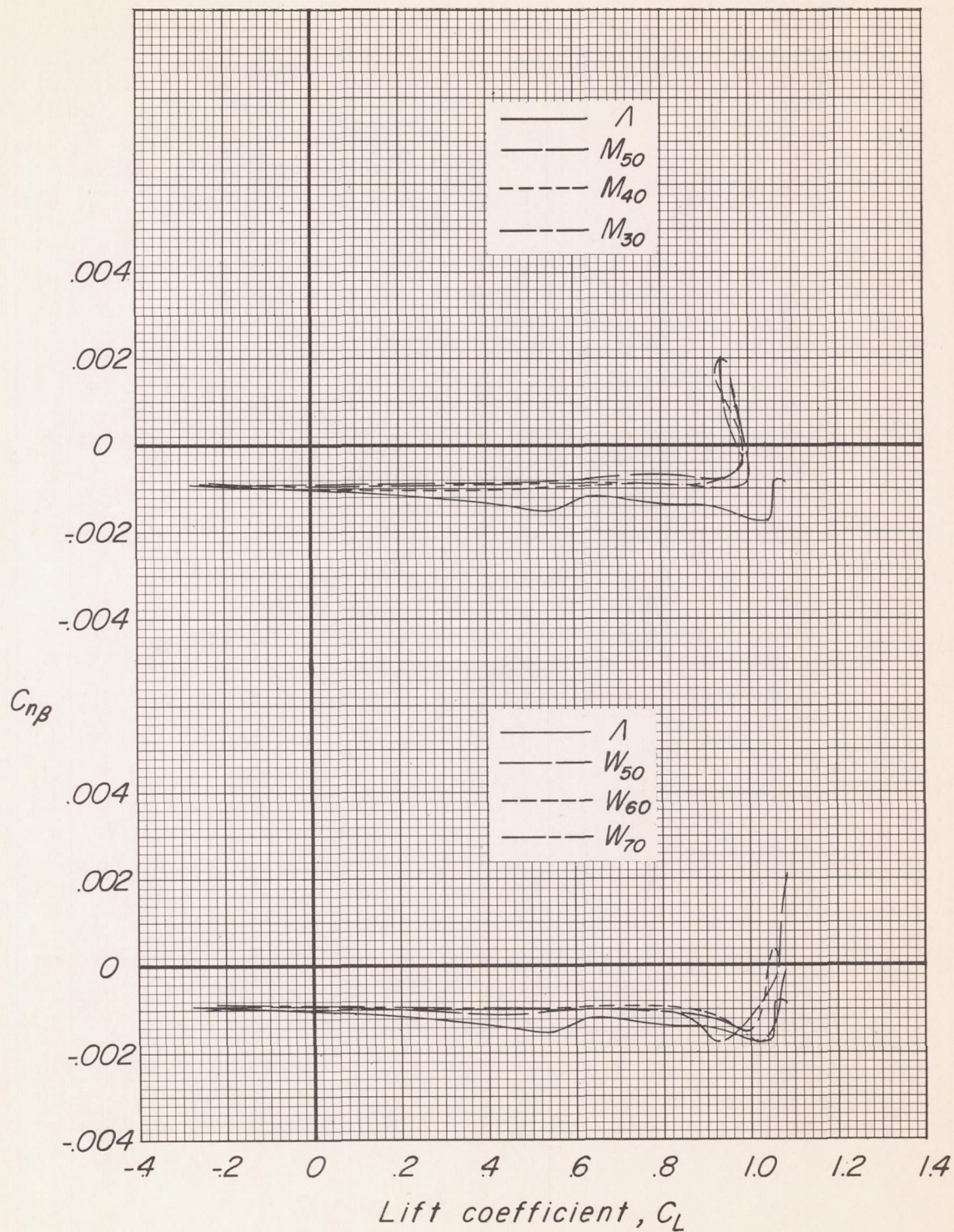
Figure 13.- Concluded.

—□— Experimental
○ Theory, ref. 6



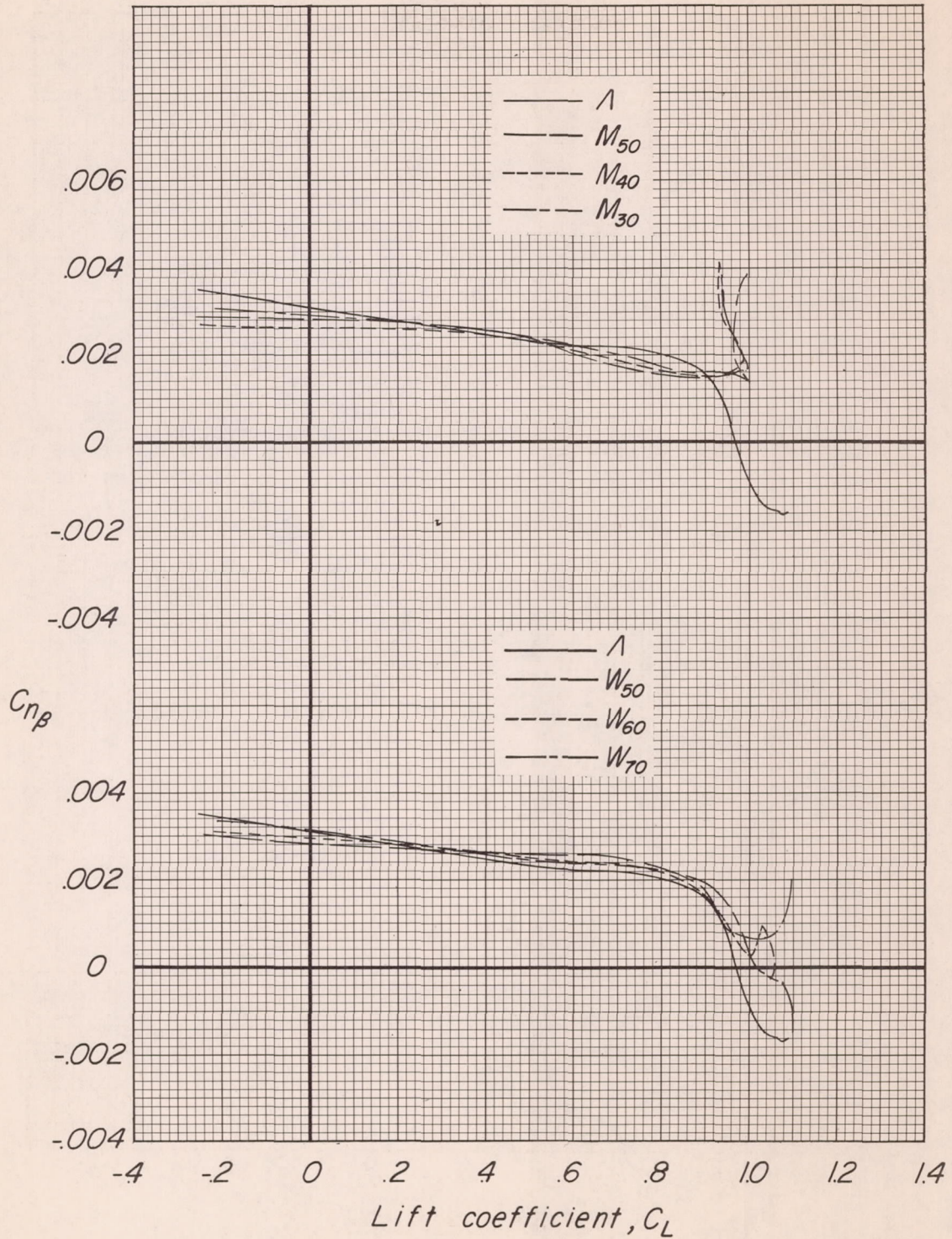
CONFIDENTIAL

Figure 14.- Variation of $C_l \beta C_L$ with spanwise location of sweep discontinuity WF.



(a) WF.

Figure 15.- Effect of spanwise location of sweep discontinuity on yawing moment due to sideslip.



(b) WFV.

Figure 15.- Continued.

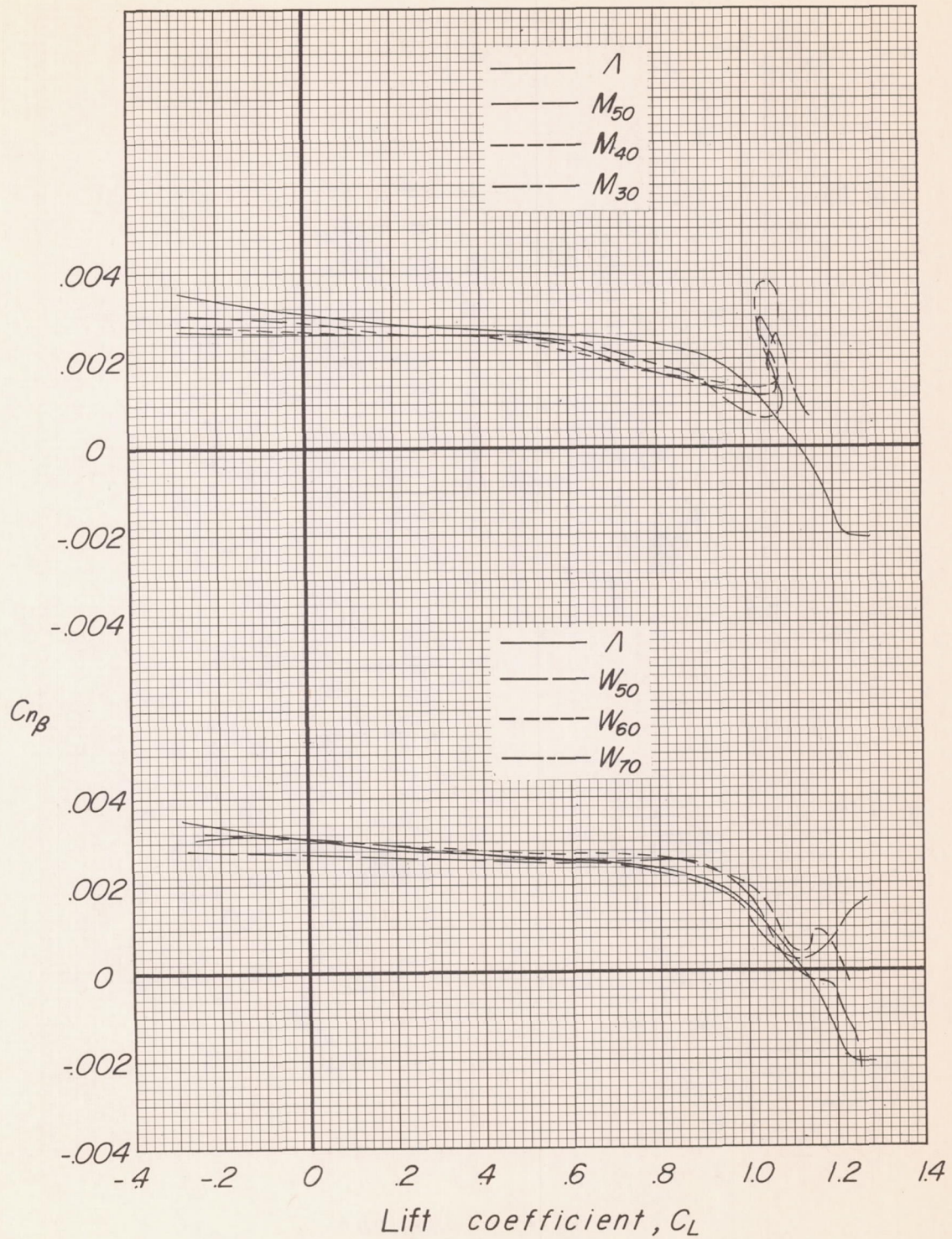
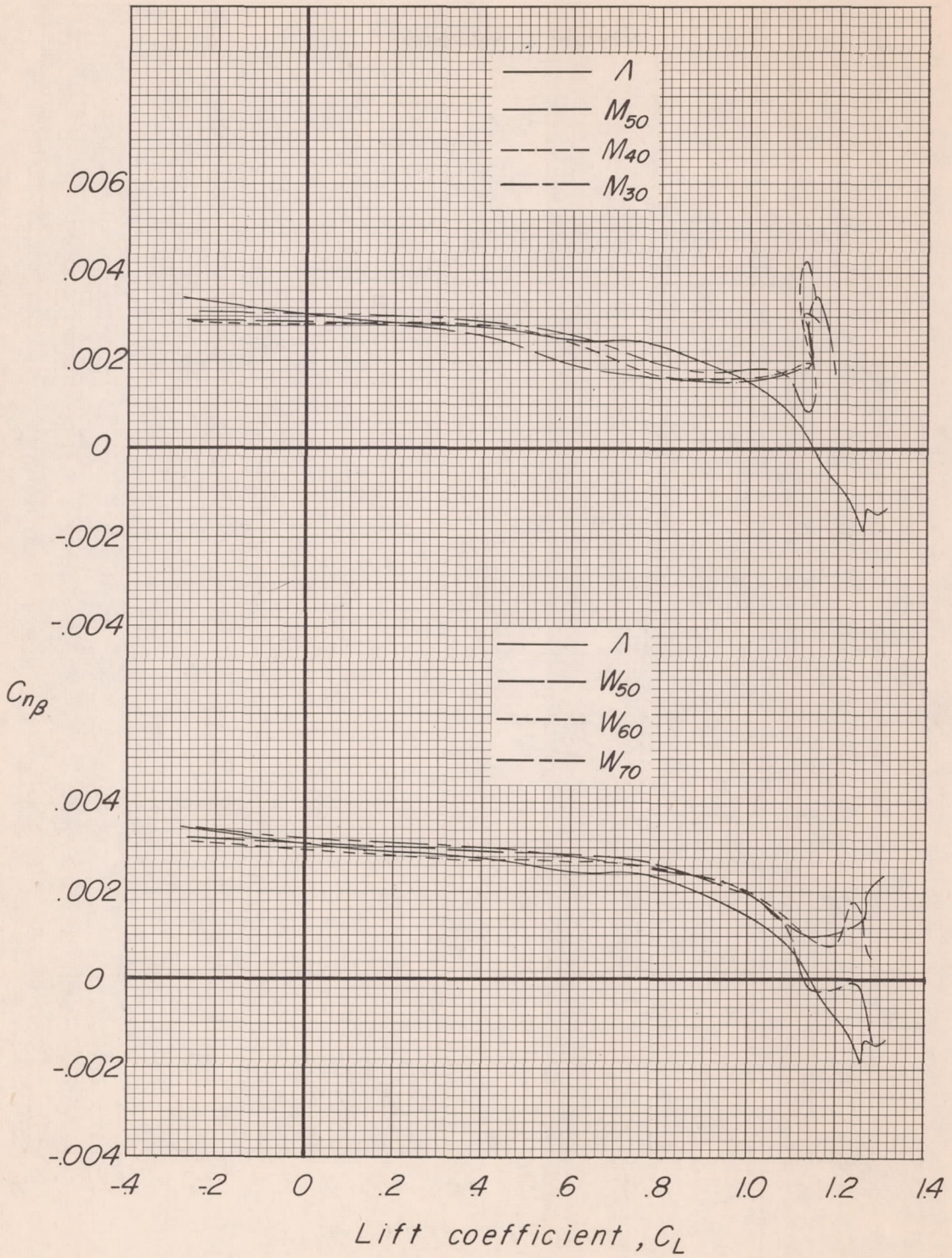
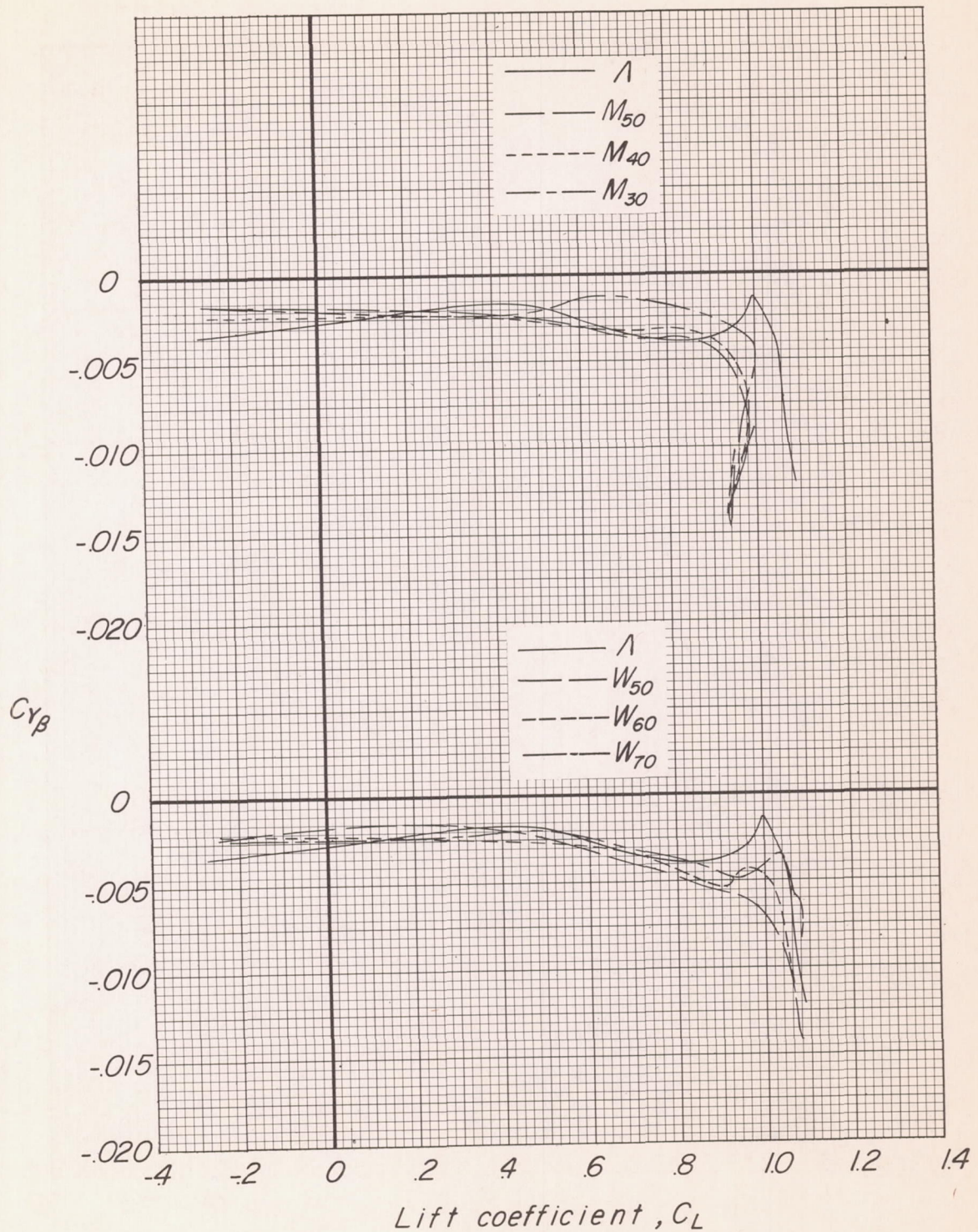
(c) W_{FVH_H}.

Figure 15.- Continued.



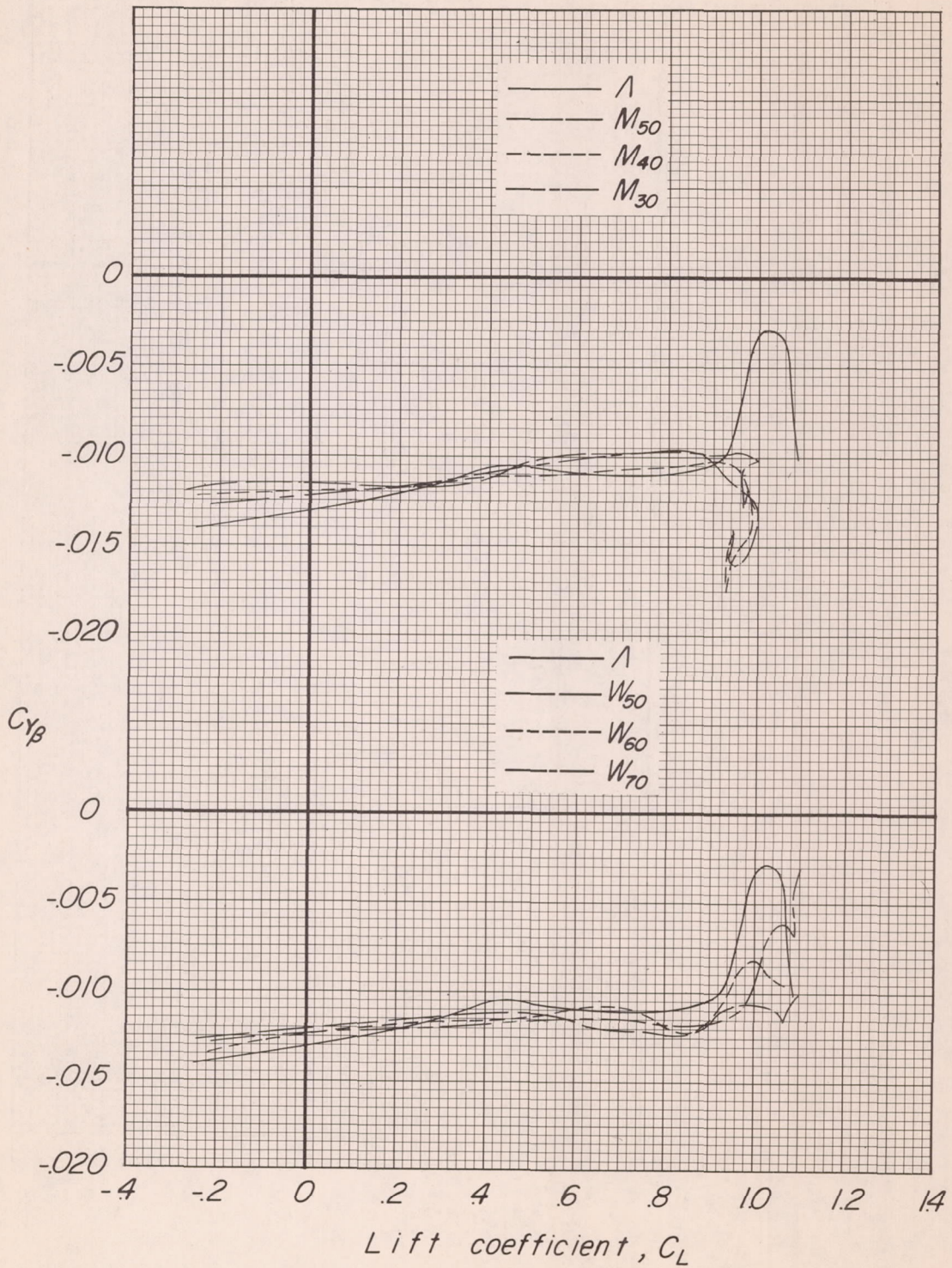
(d) W_{FVH_L}.

Figure 15.- Concluded.



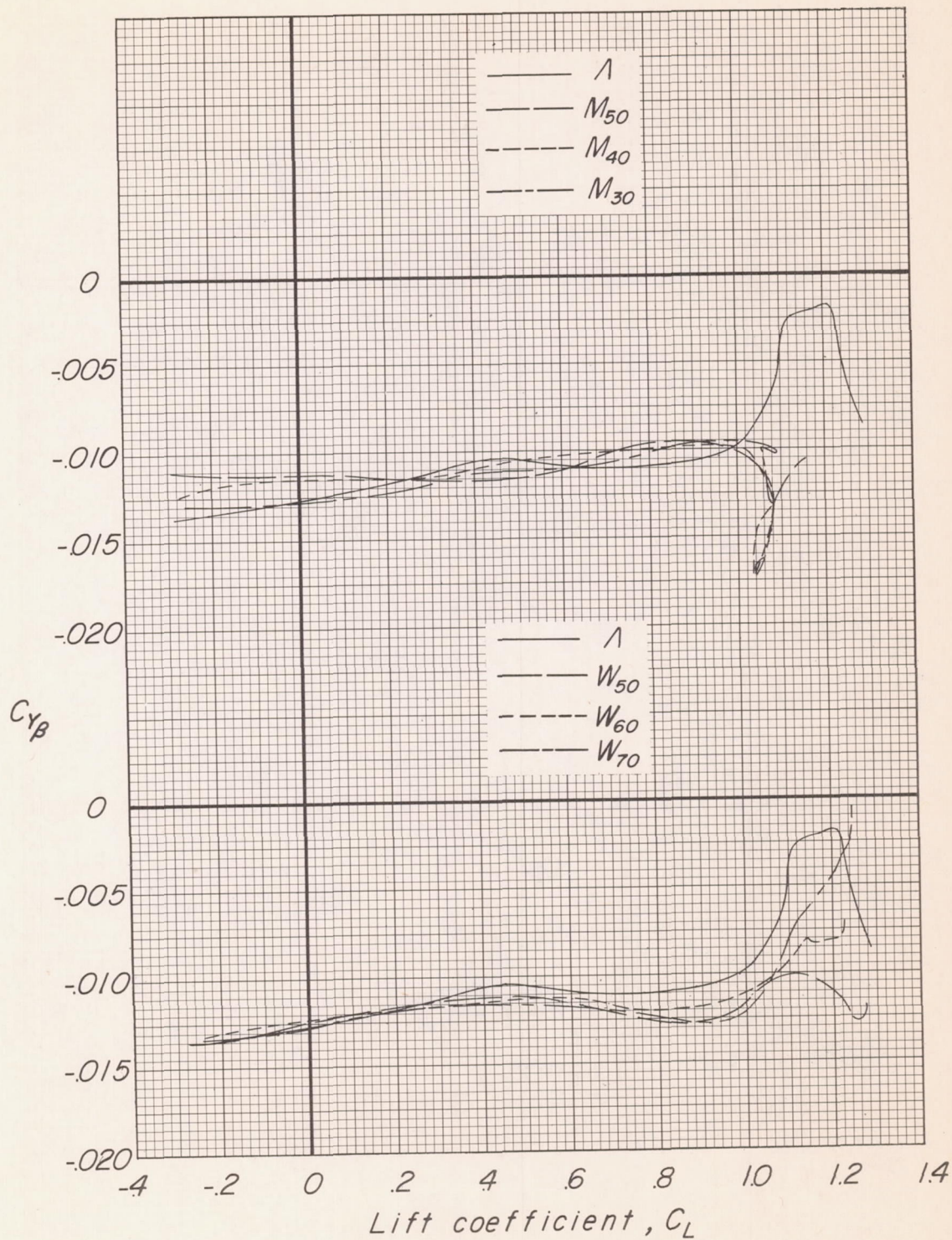
(a) WF.

Figure 16.- Effect of spanwise location of sweep discontinuity on lateral force due to sideslip.



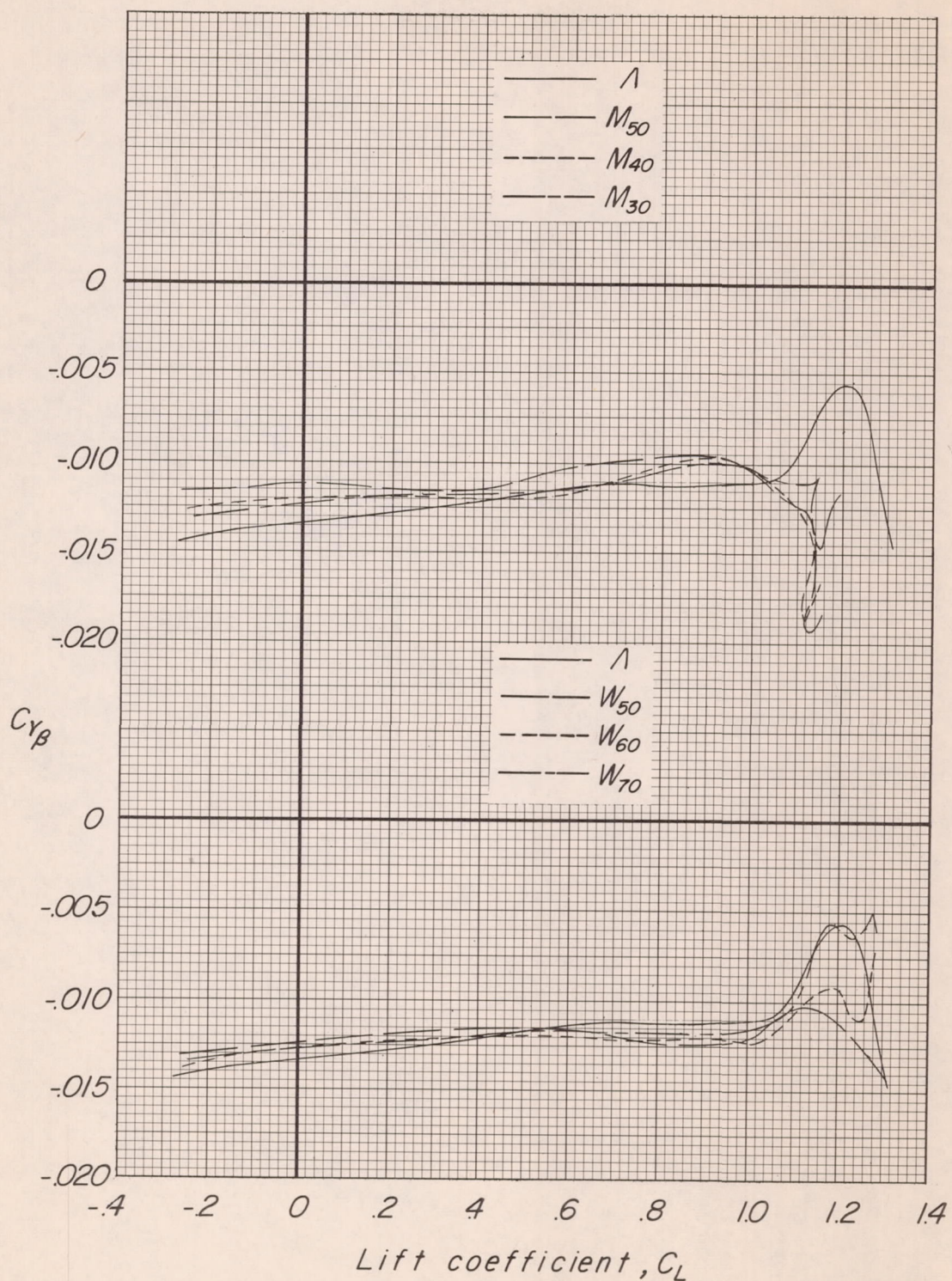
(b) WFV.

Figure 16.- Continued.



(c) WFVH_H.

Figure 16.- Continued.



(d) W_{FVH_L}.

Figure 16.- Concluded.